A Real-Time Imaging System for Lumber Strength Prediction

Riku Hietaniemi
Miguel Bordallo López
Jari Hannuksela
Olli Silvén

Abstract

In this article, we describe a system for machine vision–based lumber strength prediction. The system utilizes images taken from all four sides of pinewood boards. Those images are further divided into small subareas, and the local gradients inside each area are used to calculate the local grain direction. Together, these directions form the grain direction map. The grain direction map and knot features are used to predict the breaking strength of the board. Because of the high speed of production lines, we also present a parallel general-purpose graphics processing unit (GPGPU) implementation of the method to achieve real-time performance using low-cost hardware. We describe the challenges of the design on a GPU compared with a traditional central processing unit implementation. Most of the modern sawmills already have multiple camera systems in use, making the camera-based strength prediction extremely cost effective. In our experiments, an r^2 value of 0.63 was obtained between the measured strength attributes of the board and our strength prediction coefficient. The ground truth for the breaking strength was measured using destructive 3-point bending tests. Using a regular desktop computer, the described system achieves a throughput of over 50 Mpixels/s. For the parallel implementation, we provide qualitative evaluation of the results and a comparison of the computational speed on several platforms.

Nondestructive real-time strength grading of lumber is an important challenge in production lines of sawmills. Strength grading can increase the yield from raw material, and grades are required for material used in supporting structures for safety reasons. However, classifying lumber into specified strength categories is not an easy operation. Strength properties of boards with seemingly similar texture can vary considerably. On the other hand, boards that have poor visual appearance (e.g., because of unwanted color or texture on the surface) can still have a good load-carrying capacity.

Mechanical bending and sound wave testing are commonly used automatic methods to access strength grades in the lumber industry (Brashaw et al. 2009). Obviously, alternative technologies, such as microwave (Bogosanovic et al. 2010), X-ray (Schajer 2001, Oja et al. 2005), near infrared (Schimleck et al. 2002), and radio-frequency scanning (Steele and Cooper 2003), have also been sought for this task. The high operating speed of the production line, investment costs, and safety regulations are hindering the use of these systems. Today, strength grading in sawmills is typically still carried out visually by trained human experts.

One attractive option for overcoming this challenge is to use rather cheap noncontactive machine vision systems. Necessary image information is readily available for this purpose because multiple cameras are widely used in sawmills for quality control (Molder and Martens 2011). However, wood inspection requires extremely fast image processing because of the high speed of production lines. Using graphics processing units (GPUs) included in modern PCs for accelerating computationally intensive tasks provides the desired real-time performance to the vision system in a cost-efficient manner (Fung and Mann 2008).

Previous studies (Ivkovic et al. 2009) have shown that the coefficient of determination, or r^2 value, between modulus of elasticity (MOE) and breaking strength of structural lumber is around 0.5 to 0.7, depending on the measurement technique. Imaging solutions are unable to directly measure characteristics such as MOE or moisture content, but it has

The authors are, respectively, Researcher, Researcher, Professor, and Professor, Dept. of Computer Sci. and Engineering, Univ. of Oulu, Oulu, Finland (riku.hietaniemi@ee.oulu.fi [corresponding author], miguel.bordallo@ee.oulu.fi, jari.hannuksela@ee.oulu.fi, olli.silven@ee.oulu.fi). This paper was received for publication in August 2013. Article no. 13-00078.

Forest Prod. J. 64(3/4):126–133.
doi:10.13073/FPJ-D-13-00078

been shown that strength can be predicted with good accuracy using knots (Saravi et al. 2004). On the other hand, grain direction, ring width, and distance from pith have been shown to correlate with the strength properties of wood (Kretschmann et al. 2010). Usually, the effect of knots and grain has been studied separately, and only a few publications have considered camera-based strength grading (Brashaw et al. 2009). In this context, we study strength prediction using a combination of knot and grain features extracted from images instead of using them separately when medium-size to large knots are visible.

This article presents a lightweight visible light camera–based system for lumber strength prediction. The method performs a number of image preprocessing steps for measuring grain deviation around the lumber surface. The resulting grain deviation map is combined with knot features to form a strength prediction coefficient. In our experiments with Scots pine (*Pinus sylvestris*) samples, we measured r^2 values close to considerably more expensive X-ray systems by using visual features only. We also present a solution to meet real-time requirements using general-purpose computing on graphics processing units. Another asset of our method is that conventional cameras can be used, such as those already installed in the production line. These advantages allow our method to be used in sawmills either as a stand-alone solution or in combination with other techniques in order to increase the prediction accuracy further.

Background

The ability of lumber to resist loads depends on several factors. The most important ones listed in the literature are MOE, knots, density, moisture content, grain angles, ring width and distance from pith (Kretschmann 2010). Most of the listed qualities can be measured from images.

In this work, we focus on knots and grain, which make up the most important visual evidence of fiber orientation. Fiber distortion constitutes the single largest factor affecting the strength qualities of lumber (Dinwoodie 2000). Our goal is to combine visual knot and grain patterns in order to perform strength prediction fast and efficiently.

Knots

Knots alter the strength capabilities by replacing straight-grained wood, which is considered to have ultimate strength qualities. More important, knots are the main source of grain angle deviation. The effect that a particular knot has on grain growth depends not only on the size of the knot but also on the type of the knot. Each knot also produces a unique grain pattern around it. Knots can be divided to two basic types, sound (live) knots and dead knots. In addition, knots can be encased or intergrown. The latter means that the grain grows toward the knot center. With encased knots, growth rings tend to go around the knot, encasing it. Figure 1 illustrates the behavior of both types of knots.

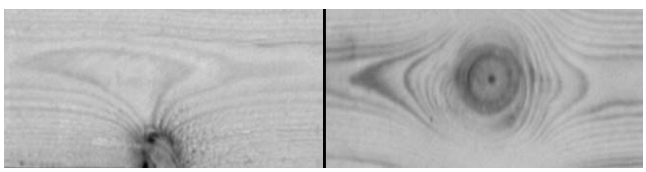

Figure 1.—Intergrown (left) and encased (right) knots.

All types of knots also prevent the even distribution of stress under load, creating local stress concentrations. This makes the board break under smaller stresses than it would without the presence of knots (Kretschmann 2010). Buksnowitz et al. (2010) compared strain fields around live and dead knots using small specimens and stated that more information about local fiber orientation is needed to increase the accuracy of strain field model.

Grain

Knots are the most visible defects in boards and arguably the single most important factor affecting the strength of wood. However, every knot produces unique interference in the grain pattern around it. This is why grain angle measurements need to be conducted when performing a strength grading.

The main reason that grain direction has an effect on the strength qualities of a board lies in the cell structure of wood. Hankinson (1921) developed a way to estimate the relationship between grain angle and strength properties of spruce that was later found to be a good estimate for other species as well (Holmberg 2000, Kretschmann et al. 2010). This relationship N can be expressed as

$$N = \frac{PQ}{P\sin^2\Phi + Q\cos^2\Phi}$$

where P is the compressive strength of wood parallel to grain, Q is the compressive strength of wood perpendicular to grain, and Φ is the angle of the grain.

Figure 2 illustrates the effect of grain angles according to Hankinson's formula for *P. sylvestris* with typical strength qualities. As we can see from the graph, even small changes in the angle between local grain and the edge of the board can have severe effects on the strength properties of the board.

Measuring grain direction is also helpful in situations where the cause of grain deviation is not visible in the image. A good example of this kind of a behavior can be seen in Figure 3, where the board is sawed next to a knot. Grain angles up to 90° are present, but the knot that is causing the deviation can be seen in only one of the two cases.

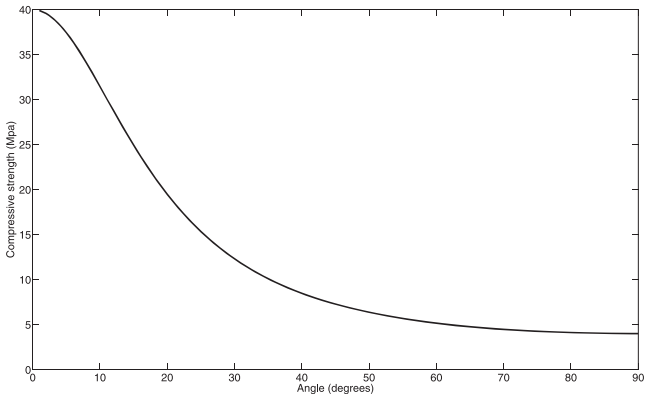

Figure 2.—Relationship between Hankinson's formula and direction of force (grain angle). Strength parallel to direction of grain is set to 40 MPa, and strength perpendicular to grain 4 MPa.

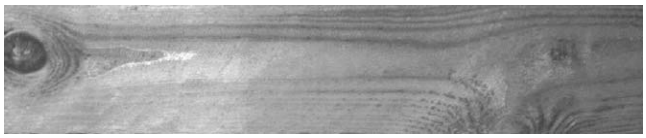

Figure 3.—Section of a board where the grain angle has changed up to 90° in both ends of the board but the knot causing the change is visible only on the left.

Related work

Nondestructive camera-based strength grading of lumber is a little-studied research area. Some earlier machine vision methods for wood grain detection, such as that of Conner et al. (1998), use images taken from the end of the log. Samarasinghe (2009) studied crack formation and propagation in wood. Grain angles, especially on the side of specimens, had a significant correlation with the crack initiation load. The test material used in this case consisted of small wooden pieces with a maximum length of 1,000 mm.

In general, knots alone can be used to assess the strength and behavior of lumber by, for example, embedding these to a finite element method model (Foley 2003). Much research has been conducted on locating and identifying knots using machine vision (e.g., Gu et al. 2010). Niskanen and Silvén (2007) tested the relationship between ring width, grain deviation, and grain density using larger boards, 1,500 by 95 by 41 mm. A combination of grain deviation and grain density produced an r^2 value of 0.38 with measured breaking strength of the boards. The test material in their work was sawn near the core of the stem so that no large knots were present. Therefore, knots did not introduce major grain distortions, and the use of knot-based features did not provide any improvement over grain angles.

Olsson et al. (2013) used a laser scatter scanner to measure the grain deviation of spruce boards and combined this information with the MOE estimates obtained using resonance frequency testing. The addition of grain-related features greatly increased the accuracy of strength prediction in comparison to using just MOE as a predictor. For a combination of knots and grain, Bãno et al. (2011) used finite element calculations to model the effect of knots and the local grain deviation around them with very promising results.

The Strength Prediction System

Measuring grain and knot positions on the surface of lumber requires fast image processing. To be able to perform at the level of production lines, speeds up to 240 pieces per min are required. Boards can be over 6 m long, and imaging resolutions higher than 1 mm/pixel are common. This leads to requirements of up to 40 Mpixels/s in processing speed for our system. GPUs included in modern PCs provide for a cost-effective and scalable alternative to the more expensive specifically tailored systems. In this context, we have built a system with suitable algorithms and made a parallel implementation using OpenCL (Open Computing Language), which makes it practical for high-speed production lines.

Quality inspection systems are widely used in sawmills. Therefore, we utilize a knot detection algorithm embedded to an automatic grading machine in our system for providing knot size and location data (Inx Ltd. 2004). Grain measurements are performed on four long surfaces of the board, providing indirect information about the actual 3-D fiber structure. The method includes three main steps: preprocessing, grain extraction, and a grain direction map construction. Figure 4 shows a block diagram presentation of the system.

In this article, we consider only one type of wood. In case of multiple species, the starting point of the algorithm needs to be the identification of the species at hand. By doing this, the inherent differences in density between species can be accounted for. Also, the effect of knots and other defects may vary between different types of wood.

Preprocessing

In the preprocessing step, all four images are divided into M by N subareas. Each subarea is median filtered before gradient calculations. A 3 by 3 mask is used for the filtering. Median filtering has two important properties that are relevant for our application. First, it reduces noise in our test images, and second, it preserves edges, which are highly related to grain patterns.

In the real-time implementation, only one memory transfer between the central processing unit (CPU) and the GPU is required because the same input image is processed in several stages. The typical pipelined design of the general-purpose (GP) GPU transfers can hide the memory transfers because the copy of the data can be done concurrently with the processing. Once the image is on the global GPU memory, the median filter algorithm can be easily parallelized by executing one thread per pixel. The median value inside the subarea/mask is computed using a divide-and-conquer approach with a binary search. The use of texture memory reduces the GPU global memory accesses, maximizing the performance since accessing the texture memory is up to 100 times faster than accessing the global memory.

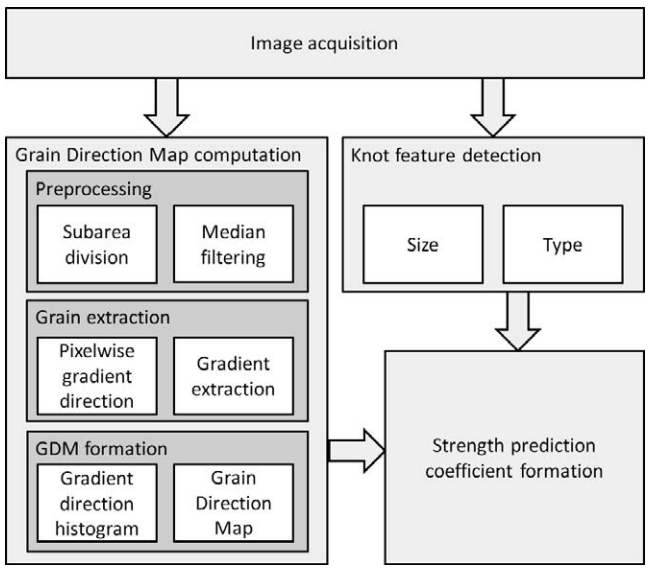

Figure 4.—A block diagram of the described system. "Grain direction map computation" block includes all the algorithms and principles described in this article.

Grain extraction

The gradient direction for every pixel is calculated in a range of [0–π] instead of [0–2π]. By doing this, we can remove the effect of the upper and lower edges of single growth rings ''competing'' with each other. This phenomenon is further explained in Figure 5.

The gradient image can be computed efficiently by convolving the original image with a filter. For this purpose, we selected 3 by 1 and 1 by 3 masks that measure the change of intensity of every pixel in the vertical and horizontal directions. These values are combined to obtain the direction of the intensity change and its magnitude. In the same way as the previously described median filtering, the GPU computation of the gradient uses texture memory to minimize global memory access and increase kernel performance.

Grain direction map computation

Inside every subarea, we calculate the gradient histogram using pixelwise gradients that are within set limits in the *y* and *x* directions. Limits are set locally for every subarea as a fraction of maximum absolute gradient value. Local limits are used to lower the effect of illumination variations and other unwanted phenomena. In our tests, we obtained the best results by setting the limit in the *x* direction approximately 1.5 times larger than in the *y* direction.

For the final histogram formation, the gradient magnitudes of the pixels that passed the limit check were not used. Instead, all pixels were treated equally and given a weight of 1. The gradient direction with the largest bin count in the histogram was chosen to be the local grain direction in that particular subarea. If two of the bins were tied for the greatest count, angles corresponding to the bins were compared. If the angles were near each other (distance is less than 2π per bin count), the result for that subarea was the average of the angles. Otherwise, that subarea was not taken into consideration. This prevents areas with no consistent gradient (and not likely to contain grain patterns) from interfering with the results. In our tests, we found that the performance of the system started to decline when the bin count was increased beyond 16. All local directions of all four sides together form a grain direction map. Figure 6 shows an example of part of such a map.

An image histogram is usually computed as a sequential algorithm that loops through the pixels of an image serially to generate the histogram results. However, the straightforward parallelization of this loop results in the updating of a highly contended memory address, with thousands of threads trying to write to one histogram array. To avoid memory writing conflicts, atomic operations are used, an approach that yields poor performance. A typical solution to this issue tries to reduce the contention on the histogram data by breaking the image into tiles that can be processed to generate a partial histogram, which can be appropriately merged at a later stage.

However, in our particular case, since our algorithm needs to compute a histogram on each one of the subareas of the image grid, the merging stage can be avoided if the the partial histograms are computed in a way that matches our designed grid. Because the typical image grid contains reasonably small pixel blocks, the computation of the partial histograms can be done using only shared memory, increasing the memory throughput and improving the overall performance (Hwu 2011).

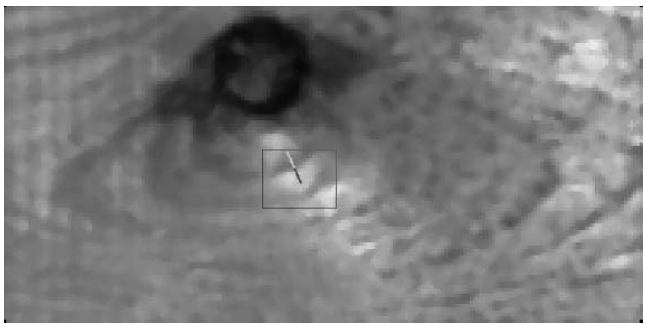

Figure 5.—Both grain angle normals (light and dark gray lines inside the square) correspond to the same local grain direction.

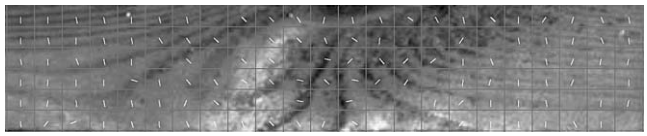

Figure 6.—An example of a grain direction map produced by our method. Light gray lines represent normals of local grain directions.

Experiments and Results

In this section, we evaluate our system using grain and knot features for predicting lumber strength. The results are compared with the ground-truth data, which were obtained using destructive bending tests. In addition, we show the computational performance and system scalability of our implementation.

Test material

The test material consisted of 194 pine boards (*P. sylvestris*) with dimensions of 3,900 by 100 by 50 mm. The board images were taken from an area approximately 50 cm long around the cylinder that was used to apply force on the board. The resolution of images was approximately 0.5 mm of board per pixel. The imaged area was assumed to be the critical area where the board was most likely to break. The modulus of rupture (MOR) of the boards was measured using a destructive 3-point bending test with a support span of 2 m. The rate of loading was increased approximately 700 N/s until breakdown. Moisture content for the boards varied between 9.0 and 13.6 percent. Distribution of MOR

Table 1.—Distribution of modulus of rupture (MOR) and density for the test material.

Feature	Value
MOR (MPa)	
Minimum value	8.1
Maximum value	71.7
Mean value	37.1
SD	13.0
Density (kg/m^3)	
Minimum value	397
Maximum value	628
Mean value	492
SD	37

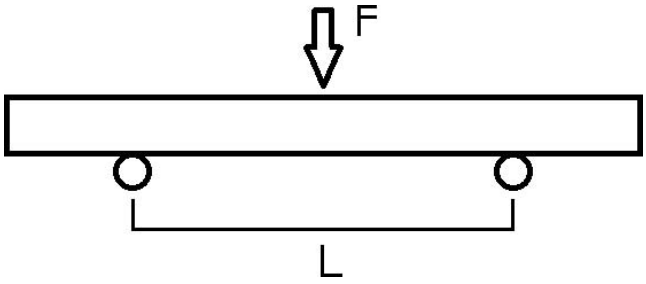

Figure 7.—Test setup for destructive testing. Mechanical cylinder was used to apply breaking force F to the middle top part of the board (3-point bending test). Support span L of 2 m was used.

as well as the density for test material can be seen in Table 1. Figure 7 shows the test setup used.

All knot-based information used in this work was extracted with a knot detection algorithm integrated to the quality measurement timber inspection system (Inx Ltd. 2004). Boards were sawn near the stem core. Therefore, almost all the knots in the test material had smaller ends of similar sizes for the reason that knots originate from the core and grow outward toward the bark in the shape of a cone. All knot sizes mentioned later refer to the size of the larger end of the knot.

Strength prediction tests

Using grain angles only.—Grain angle, or slope of grain, is usually measured using 1-inch (25-mm) intervals (Kretschmann 2010). In our tests, we achieved good results using much smaller sections (subarea size corresponding to a 10-mm section of the board giving the best results). The final area used for prediction depends also on the number of subareas used. Figure 8 illustrates the ratio between prediction accuracy for the best found feature and number of subareas. The best result is achieved using 17 subareas, corresponding to an approximately 170-mm-long section of a board.

Every local grain direction in the grain direction map is compared with the edge of a board, which is equal to calculating the absolute difference between the local grain angle and 0. By doing this for every subarea, grain direction maps are transformed to grain deviation maps. In grain deviation maps, there is a single value for every subarea that corresponds to the difference between straight grain (0° angle) and the local grain direction.

Table 2 lists the values for some of the best single grain features. The best grain feature found was the maximum sum of grain deviations calculated around the board, using all four of the available images, achieving an r^2 value of 0.54. Using all four sides clearly offers improvement over using only one side. The r^2 value for the single most significant side, which in our case was the top part of the board, was 0.46.

We also compared the gradient histogram method with another popular method for local direction estimation using directional Gaussian filters (Gizatdinova and Surakka 2006). Using the directional filters produced weaker grain direction maps, with an r^2 value of 0.40 when compared with the actual breaking strength.

Using knot features only.—Using the knot size as a feature is difficult when combined with other features because of scaling. For example, the angle between the edge of the board and the grain can have values only between [0–π], so it can be easily scaled to [0–1]. We found that scaling the area of the knot using the corresponding area on the flat side of the board produced good results with our test material. The scaling is illustrated in Figure 9. Because the ratio between the areas for a rectangle and a circle is not 1, the scaled knot size (SKS) is multiplied by a coefficient equal to the ratio. All knots are considered as circles instead of ellipses, adding some error to the equation. Using this technique, we found that the r^2 value for the single largest knot explaining the variation in strength increased from 0.41 to 0.46, a result that we achieved in our previous studies (Hietaniemi et al. 2011).

Usually, scaling for knots is done using the knot area ratio (KAR; Ozelton and Baird 2006). It is calculated as the ratio between the cross-sectional areas of a board and a knot. In this case, using the KAR produced weaker results. Table 3 shows the values for single knot–based features. We found experimentally that a good way to compensate for the knot type (dead/live) was to divide the knot size by a factor of 2.

Table 2.—r^2 values for the grain-based features.

Feature	r^2 value
Maximum grain deviation sum, all four images (Msum4)	0.54
Maximum grain deviation sum, one image (top) (Msum1)	0.46
Mean grain angle, all four images (MGA)	0.34
Msum4, directional Gaussian filters	0.40

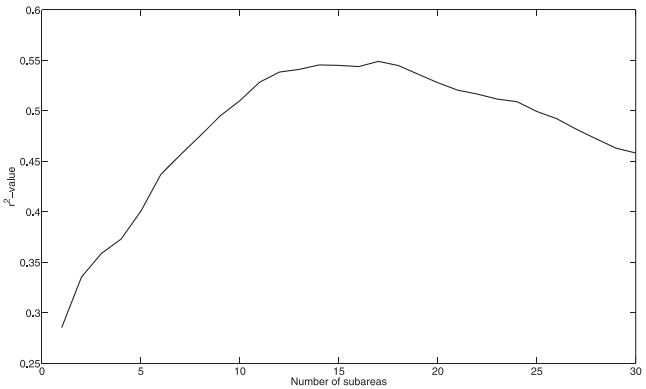

Figure 8.—r^2 value for the maximum grain deviation sum, all four images (Msum4), plotted against the number of subareas.

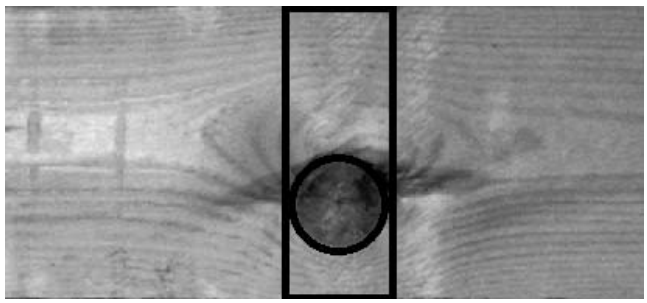

Figure 9.—The area of the knot (circle) is normalized by the area of the height of the board times the diameter of the knot (square).

Table 3.—r^2 values for the knot size–based features.

Feature	r^2 value
No type compensation	
Scaled knot size	0.37
Knot size	0.35
Knot area ratio	0.18
Type compensation	
Scaled knot size	0.46
Knot size	0.40
Knot area ratio	0.27

Table 4.—r^2 values for different grading solutions.

Solution	r^2 value
Our combined method	0.63
Our grain features	0.54
MOE[a] (bending test, our material)	0.75
Ring width (Niskanen and Silvén 2007)	0.35
Grain deviation and density (Niskanen and Silvén 2007)	0.38
Grain deviation and resonance frequency (Olsson et al. 2013)	0.71
X ray (Schajer 2001)	0.68–0.78
X ray and MOE (Oja et al. 2005)	0.56

[a] MOE = modulus of elasticity.

Using this compensation improved the coefficient of determination for both the KAR and the SKS.

Using both knot and grain features

The best overall performance was achieved by combining Msum4 (maximum grain deviation sum, all four images) with SKS. Figure 10 shows the strength reduction coefficient formed using these two features plotted against the MOR of the boards. The r^2 value was 0.63. Both of the features (Msum4 and SKS) are first scaled to [0–1] and then simply added together to form a strength prediciton coefficient ranging from [0–2].

Comparison of our results to those previous grain-related studies, as well as similar types of strength grading, can be seen in Table 4. The coefficient of determination between MOE and MOR for our test material is also shown.

Based on the data in Table 4, the performance level of camera-based strength grading is in the same range as X-ray–based methods. It should be noted, though, that the test material was of a different subspecies of pine in Schajer (2001) and Oja et al. (2005). Grain deviation in Olsson et al. (2013) was measured using a laser scanner instead of a conventional camera. Also, the MOE was expected to be known everywhere in the board and was measured using a resonance frequency technique. The tested species in this case was spruce.

Computational performance

Performance of the GPU.—The real-time implementation was done using only low-budget commercially available hardware and software tools. The reference platform for our implementation was a Samsung R580 laptop computer with an Intel i5-M450 Quad-core processor and an nVidia GT330M GPU. The comparative performance of the different stages of the gradient map computation algorithm for HD1920 (1,900 by 1,080) resolutions can be seen in Table 5.

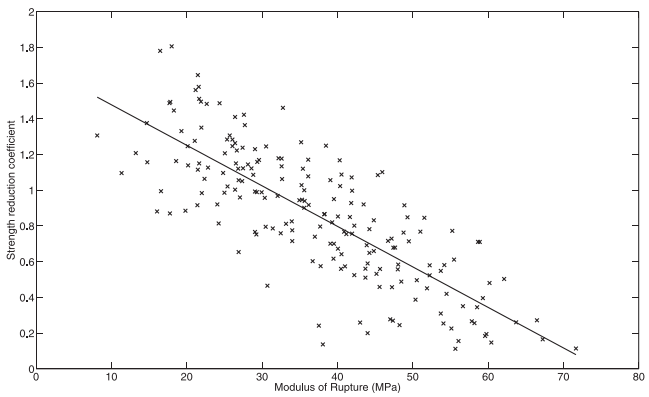

Figure 10.—Maximum grain deviation sum, all four images, plus scaled knot size plotted against the modulus of rupture of the board.

As Table 5 shows, there is a massive difference in processing speed for our system between the CPU and the GPU implementation. The reference CPU implementation uses the same OpenCL code as the GPU system, which is able to take advantage of the multicore architectures. Although the optimized CPU offers a big improvement over a nonoptimized Matlab implementation, its 1.2-Mpixel/s throughput is not sufficient for real-time computation on a high-speed production line. On the other hand, the GPU implementation achieves a remarkable throughput while keeping the CPU load under the 25 percent mark, which could be used for other tasks.

System scalability.—When deploying a lumber inspection camera system in a production line, the scalability of the solution is of great importance. The use of GPGPU calculations offers an easy way to tailor the computational system for the exact needs of the facility and helps avoid any excessive investments. On the other hand, if computational needs increase over time, upscaling can be done conveniently. A system that proves to be scalable with the number of processors can be implemented in a modular way. This allows the easy introduction or dropping of new cameras and computational units that could be independent or embedded in the cameras themselves. In this context, we implemented and tested our software on several commercially available platforms, including CPUs and GPUs. Table 6 shows the computation speed of an HD1920 frame in three different systems—a desktop computer, a laptop, and a tablet PC—all in the same price range.

Table 5.—Performance comparison of the several implementations of the algorithms.

	Intel Quad core		nVidia GT330M
	Matlab	OpenCL[a]	OpenCL
Data input/output (ms)	0	0	0.008
Median filter (ms)	4,829	1,335	59
D gradient (ms)	1,268	354	11
Histograms (ms)	207	59	12
Total time (ms)	6,304	1,748	90
Speedup	0.28×	1×	20×
Throughput (Mpixels/s)	0.33	1.2	23

[a] OpenCL = Open Computing Language.

Table 6.—Performance of the algorithm in different system cards.

System	Dell Inspiron	Samsung R580	Acer Iconia W500
Format	Desktop	Laptop	Tablet
CPU model[a]	Intel i5 3.4 GHz	Intel i5m 2.4 Ghz	AMD C-50 1 GHz
No. of cores	4	4	2
GPU model[b]	GT620	GT330M	Radeon HD 6250
No. of cores	96	48	80
Power consumption (W)	112 (CPU) + 49 (GPU)	35 (CPU) + 23 (GPU)	5 (CPU) + 4 (GPU)
Shader clock frequency (MHz)	1,400	1,265	280
Processing time (ms)			
CPU	1,133	1,748	7,950
GPU	40	90	243
Speedup factor, GPU/CPU	28×	20×	33×
Input/output time (ms)	14	10	0
Energy (J/Mpixels)			
CPU	61	52.5	25
GPU	0.9	1.0	0.47
Maximum throughput (Mpixels/s)	53.6	24.5	8.7

[a] CPU = central processing unit.
[b] GPU = graphic processing unit.

It has been found that the computation process is memory bound and that data transfer can be done in parallel with the processing. Therefore, the use of a GPU with more stream processors or cores leads to an increment of speed almost proportional to the number of them added.

The results show that a mid-budget laptop GPU is able to compute the lumber strength with a throughput higher than 20 Mpixels/s, an amount that can be doubled with the use of a regular desktop computer, such as the low-budget Dell Inspiron 660. However, the GPU model and the OpenCL implementation enable the integration of the system in smaller processors, such as the AMD C-50 APU (GPU + CPU) included in the Acer Iconia tablet PC. Its small footprint processor offers moderately good throughput while keeping the energy consumption and heat dissipation very low. These processors can be also integrated in an autonomous smart-camera device (Ximea Ltd. 2013) that could be easily deployed in any kind of production line. It is also easily scalable simply by adding extra camera devices.

Conclusions

In this article, we have presented a real-time camera-based system for grain angle deviation measurement utilizing modern GPGPU computation. Using the maximum grain deviation sum, calculated from all four sides of the board, produced an r^2 value of 0.54 when compared with the measured MOR of the boards. When the scaled size of the largest knot was added, the r^2 value increased to 0.63. Throughput up to 53.6 Mpixels/s was achieved using a common workstation.

The main advantage of this system is that it can be added to modern sawmills with very low investment, and the running costs are minimal. This kind of a system makes it possible for even the smallest of companies to have easy access to strength grading and to improve their profitability. On the downside, when compared with the most advanced X-ray systems, the strength prediction accuracy is slightly weaker. However, even if some other strength grading system is already installed in the sawmill, our system can be added as an additional module to improve the overall accuracy of the grading.

As a stand-alone system, the strength prediction accuracy can be increased with future work. The distance from the pith of the tree as well as ring width and density may be used to increase the accuracy of strength prediction. More information about knots, such as location, can be taken into account. The ratio of juvenile and mature wood can also be estimated from images.

The grain direction maps themself are not perfect. Some local directions are based not on the direction of grain but rather on some other phenomena. Disturbances such as strong reflections and overexposure, as well as dirt and similar, strong gradient-inducing effects, cause errors in the maps. Eliminating these errors will help increase the accuracy of grain direction maps, thus increasing the strength prediction accuracy. Good imaging conditions with constant lighting will ensure good-quality maps.

The strength prediction coefficient was formed in a very straightforward way by scaling the used features (knot size and grain deviation sum) to [0–1] and adding them together. For future research, other, more advanced methods of combining information should be considered.

Literature Cited

Bãno, V., F. Arriaga, A. Soilán, and M. Guaita. 2011. Prediction of bending load capacity of timber beams using a finite element method simulation of knots and grain deviation. *Biosyst. Eng*. 109(4):241–249.

Bogosanovic, M., A. Al Akbunky, and G. Emms. 2010. Overview and comparison of microwave noncontact wood measurement techniques. *J. Wood Sci*. 56:357–365.

Brashaw, B., V. Bucur, F. Divos, R. Goncalves, J. Lu, R. Meder, R. Pellerin, S. Potter, R. Ross, X. Wang, and Y. Yin. 2009. Nondestructive testing and evaluation of wood: A worldwide research update. *Forest Prod. J*. 59:7–14.

Buksnowitz, C., C. Hackspiel, K. Hofstetter, U. Müller, W. Gindl, A. Teischinger, and J. Konnerth. 2010. Knots in trees: Strain distribution in a naturally optimised structure. *Wood Sci. Technol*. 44:389–398.

Conner, W., R. Schowengerdt, M. Munro, and M. Hughes. 1998. Design of a computer vision based tree ring dating system. *In:* IEEE Southwest Symposium on Image Analysis and Interpretation, April 5–7, 1998, Tucson, Arizona. pp. 256–261.

Dinwoodie, J. 2000. Timber: Its Nature and Behaviour. Taylor & Francis, London.
Foley, C. 2003. Modeling the effects of knots in structural timber. PhD thesis. Lund University, Sweden.
Fung, J. and S. Mann. 2008. Using graphic devices in reverse: GPU-based image processing and computer vision. *In:* IEEE International Conference on Multimedia and Expo, June 23–26, 2008, Hannover, Germany. pp. 9–12.
Gizatdinova, Y. and V. Surakka. 2006. Feature-based detection of facial landmarks from neutral and expressive facial images. *IEEE Trans. Pattern Anal. Machine Intelligence* 28(1):135–139.
Gu, I., H. Andersson, and R. Vicen. 2010. Wood defect classification based on image analysis and support vector machines. *Wood Sci. Technol*. 44:693–704.
Hankinson, R. L. 1921. Investigation of crushing strength of spruce at varying angles of grain. Air Force Information Circular No. 259. US Air Service, Washington, D.C.
Hietaniemi, R., J. Hannuksela, and O. Silvén. 2011. Camera based lumber strength classification system. *In:* Proceedings of 12th International Conference on Computer Vision Applications (MVA 2011), Nara, Japan. pp. 251–254.
Holmberg, H. 2000. Influence of grain angle on Brinell hardness of Scots pine (*Pinus sylvestris* L.). *Holz Roh- Werkst*. 58(1–2):91–95.
Hwu, W.-m. W. (Ed.) 2011. GPU Computing Gems Emerald Edition. Vol. 1. Morgan Kaufmann, Burlington, Massachusetts.
Inx Ltd. 2004. Optigrader. Inx Ltd., Finland.
Ivkovic, M., W. Gapare, A. Abarquez, J. Ilic, M. Powell, and H. Wu. 2009. Prediction of wood stiffness, strength and shrinkage in juvenile wood of radiata pine. *Wood Sci. Technol*. 43:237–257.
Kretschmann, D. 2010. Mechanical properties of wood. *In:* Wood Handbook. General Technical Report FPL-GTR-190. USDA Forest Service, Forest Products Laboratory, Madison, Wisconsin. Chap. 5, pp. 5-1–5-46.
Kretschmann, D., J. J. Bridwell, and T. C. Nelson. 2010. Effect of changing slope of grain on ash, maple, and yellow birch bending strength. Paper No. 716. *In:* Proceedings of the 11th World Conference on Timber Engineering, June 20–24, 2010, Riva del Garda, Trento, Italy.
Molder, A. and S. Martens. 2011. Image processing in the woodworking industry: Challenges, solutions and platforms. *Electron. Electrical Eng*. 113(7):43–46.
Niskanen, M. and O. Silvén. 2007. Machine vision based lumber grain measurement. *In:* Proceedings of the IAPR Conference on Machine Vision Applications (MVA 2007), May 16–18, 2007, Institute of Industrial Science, University of Tokyo, Tokyo. pp. 408–411.
Oja, J., B. Källsner, and S. Grundberg. 2005. Predicting the strength of sawn wood products: A comparison between x-ray scanning of logs and machine strength grading of lumber. *Forest Prod. J*. 55:55–60.
Olsson, A., J. Oscarsson, E. Serrano, B. Källsner, M. Johansson, and B. Enquist. 2013. Prediction of timber bending strength and in-member cross-sectional stiffnes variation on the basis of local wood fibre orientation. *Eur. J. Wood Wood Prod*. 71(3):319–333.
Ozelton, E. and J. Baird. 2006. Timber Designers' Manual. John Wiley & Sons, New York.
Samarasinghe, S. 2009. Exploration of fracture dynamics properties and predicting fracture toughness of individual wood samples using neural networks. *Silva Fenn*. 43(2):275–239.
Saravi, A., P. Lawrence, and F. Lam. 2004. Implementation of a mechanics-based system for estimating the strength of timber. *IEEE Trans. Instrument. Meas*. 53(2):284–292.
Schajer, G. 2001. Lumber strength grading using x-ray scanning. *Forest Prod. J*. 51:43–50.
Schimleck, L., R. Evans, and A. Matheson. 2002. Estimation of D. Don clear wood properties by near-infrared spectroscopy. *J. Wood Sci*. 48:132–137.
Steele, P. and J. Cooper. 2003. Estimating lumber strength with radio frequency scanning. *Comput. Electron. Agric*. 41(13):77–83.
Ximea Ltd. 2013. GPU accelerated PC camera CURRERA-G'. Ximea Ltd., Germany.